ULTRACOLD CHEMISTRY

Control of reactive collisions by quantum interference

Hyungmok Son[1,2]*, Juliana J. Park[1], Yu-Kun Lu[1], Alan O. Jamison[3], Tijs Karman[4], Wolfgang Ketterle[1]

In this study, we achieved magnetic control of reactive scattering in an ultracold mixture of ^{23}Na atoms and ^{23}Na^{6}Li molecules. In most molecular collisions, particles react or are lost near short range with unity probability, leading to the so-called universal rate. By contrast, the Na + NaLi system was shown to have only ~4% loss probability in a fully spin-polarized state. By controlling the phase of the scattering wave function via a Feshbach resonance, we modified the loss rate by more than a factor of 100, from far below to far above the universal limit. The results are explained in analogy with an optical Fabry-Perot resonator by interference of reflections at short and long range. Our work demonstrates quantum control of chemistry by magnetic fields with the full dynamic range predicted by our models.

Advances in cooling atoms and molecules have opened up the field of quantum scattering resonances (*1*–*4*) and ultracold chemistry (*5*, *6*). At micro- and nanokelvin temperatures, collisions occur only in the lowest partial wave, and the collisional physics can be reduced to a few well-defined parameters, which, in many systems, are the s-wave scattering length and a two-body loss-rate coefficient. Collisions involving molecules are often much more complex, owing to the strong anisotropic interaction at short range and multiple decay channels including reactions (*7*–*10*). One goal of current research is to identify systems that can still be understood with relatively simple models, including the model of universal rate coefficients (*11*), as well as single-channel and two-channel models. Such systems are most likely to enable researchers to achieve controllable quantum chemistry in which the outcome of reactions is steered by external electromagnetic fields (*12*, *13*).

Collisions in molecular systems can be described by the reflection of the wave function in two regions. At long range, the attractive van der Waals (vdW) potential acts as a highly reflective mirror, owing to quantum reflection in low-temperature scattering (Fig. 1). When the colliding particles are in close proximity, they can again be reflected by the repulsive short-range potential, or they can get lost because of reactions and/or inelastic transfer to other states. These losses can be represented by transmission through the short-range mirror (Fig. 1). In the universal limit, the transmission is 100%, and the entire incoming flux is lost.

Most ultracold molecular collisions studied thus far have loss-rate coefficients at or close to the universal value (*14*–*25*). However, when partial reflection occurs at short range, the resulting loss rate can be higher or lower than the universal value, depending on the interference created by multiple reflection pathways. This fact is analogous to an optical Fabry-Perot interferometer. This optical analog fully captures the results of a single-channel description of reactive molecular collisions (*11*, *26*). We extended the single-channel model by adding a Feshbach resonance as a lossless phase shifter that can tune between constructive and destructive interferences.

Our experimental system, which consists of collisions of triplet ro-vibrational ground-state NaLi with Na near 978 G, is fully described by this Fabry-Perot model. We saw loss rates that exceeded the universal rates by a factor of ~5, tunable via a Feshbach resonance over a range of more than two orders of magnitude. We have also characterized a weaker loss resonance, where the phase shifter was "lossy"—i.e., the closed channel of the Feshbach resonance had a short lifetime and dominated the loss, almost completely spoiling the quality factor of the Fabry-Perot resonator. This resonance has to be described by a two-channel model with the lifetime of the bound state as an additional parameter (*27*). Our experiment has established NaLi + Na as a distinctive system that realizes the full dynamic range of recent models developed to describe reactive collisions involving ultracold molecules (*11*, *26*). Furthermore, to the best of our knowledge, this system is only the second example for which Feshbach resonances between ultracold molecules and atoms have been found (*28*, *29*).

Experimental protocol

A mixture of ~3×10^5 Na atoms and ~3×10^4 NaLi molecules in the triplet ro-vibrational ground state was produced in a 1596-nm one-dimensional (1D) optical lattice created by retro-reflecting the trapping beam. The sample was confined as an array of ~1000 pancake-shaped clouds. The atoms and molecules were both in the upper stretched hyperfine states, where all electron and nuclear spins were aligned along the bias field (*30*, *31*). This spin-polarized mixture was in a chemically stable quartet state. The sample was prepared at a temperature $T_{\mathrm{NaLi}} \approx T_{\mathrm{Na}} \sim T = 1.55$ μK, well within the regime for threshold behavior of collisions, which required the temperature to be much less than the characteristic temperature determined by the vdW potential, $T_{\mathrm{vdW}} = \hbar^2/2\mu k_{\mathrm{B}} r_6^2$ (*32*) with the vdW length $r_6 = (2\mu C_6/\hbar^2)^{1/4}$, where h is Planck's constant divided by 2π, μ is the reduced mass of NaLi and Na, k_{B} is the Boltzmann constant, and C_6 is the vdW constant for the atom-molecule potential. With C_6 = 4026 in atomic units (*33*), $T_{\mathrm{vdW}} \approx 500$ μK.

The atom-molecule mixture was initially prepared near the Na-Li Feshbach resonance at 745 G, and then the bias field was ramped to the target value in 15 ms. We determined collisional lifetimes of the atom-molecule mixture by holding the sample for a variable time at the target magnetic field, after which the field was ramped back to 745 G where the remaining molecules were dissociated and detected. The number of dissociated Li or Na atoms in the hyperfine ground state was measured by resonant absorption imaging (*30*). The hyperfine state of Na atoms from dissociation differed from that of Na atoms in the initial atom-molecule mixture.

Decay curves for the molecules are compared in the inset of Fig. 2, near and far away from the strong atom-molecule Feshbach resonance studied in this work. Our observable $\gamma(B)$ (where γ is the loss rate and B is the magnetic field) is the difference of initial loss rates of NaLi molecules with and without Na atoms. It is obtained by fitting the whole decay curve using the standard differential equations for two-body decay [see supplementary materials (SM)]. The loss in the absence of Na atoms is caused by p-wave reactive collisions between molecules. The measured molecular two-body loss-rate coefficient $\beta = 2.6(7) \times 10^{-12}$ (cm^3/s) (T_{NaLi}/μK) near 980 G is within a factor of 2 of the prediction from the universal loss model (see SM). Single-particle loss due to the vacuum-limited lifetime of >20 s was negligible.

We avoided the need for absolute sodium density measurements by comparing the measured decay rate to the decay rate of the mixture in a nonstretched spin state. Because this mixture collides on a highly reactive doublet potential, the decay was reliably predicted to occur with the s-wave universal rate coefficient, which is well known for our system (*33*). By

[1]MIT-Harvard Center for Ultracold Atoms, Research Laboratory of Electronics, Department of Physics, Massachusetts Institute of Technology, Cambridge, MA 02139, USA. [2]Department of Physics, Harvard University, Cambridge, MA 02138, USA. [3]Institute for Quantum Computing and Department of Physics and Astronomy, University of Waterloo, Waterloo, Ontario N2L 3G1, Canada. [4]Institute for Molecules and Materials, Radboud University, Heijendaalseweg 135, 6525 AJ Nijmegen, Netherlands.
*Corresponding author. Email: hson@g.harvard.edu

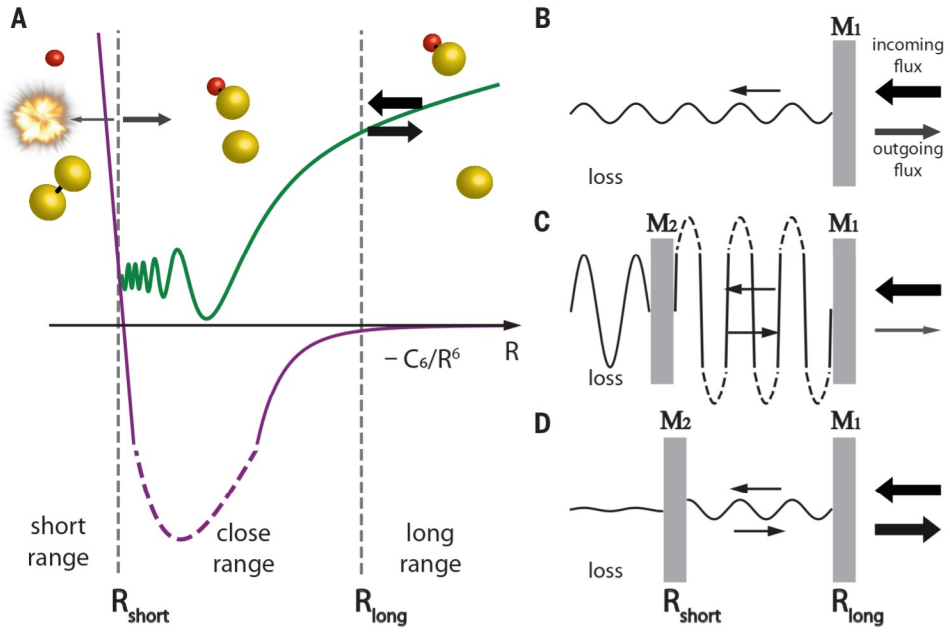

Fig. 1. Fabry-Perot interferometer model for reactive collisions. (**A**) Collisions between an atom (yellow sphere) and a molecule (yellow and red sphere together) occur in a potential that is the attractive vdW potential $-C_6/R^6$ at long range [$R > R_{long}$ (where R is the interparticle distance)] and a strongly repulsive potential at short range ($R < R_{short}$). The scattering dynamics (represented by the wave function in green) can be fully described by quantum reflection off of the vdW potential at $R \sim R_{long}$ and reflection and transmission at $R \sim R_{short}$ (*11*, *26*). Loss at close and short range is caused by the coupling of the incoming channel (in our case, a chemically stable quartet state) to a lossy channel (here, a reactive doublet state) and described by a reflectivity of <100% of the inner mirror. For instance, in the doublet state, a singlet Na_2 molecule (two yellow spheres) can be formed. This situation is fully analogous to an optical Fabry-Perot interferometer with two partially reflective mirrors (M_1 and M_2). Reactive loss is proportional to the flux transmitted through both mirrors. (**B**) Transmission through mirror M_1 only represents the universal loss. Depending on constructive and destructive interference between multiple reflections, the loss can be highly enhanced [on resonance (**C**)] or suppressed (**D**) relative to the universal loss. (C) and (D) are depicted for a reflectivity $|r_2|^2 \sim 0.89$, with 1000-fold loss enhancement between these panels.

comparing datasets taken at different times (see SM), we estimated the uncertainty of the density calibration to be ~40%.

We also measured the loss rate of the mixture in the nonstretched spin state by using the measured particle number and temperature, as well as a model for the anharmonic trapping potential. With the measurement, we have confirmed within 30% uncertainty that the rate is indeed the universal rate (see SM). Because we regard the theoretical prediction to be highly reliable, we did not use the experimental density calibration in the analysis reported here.

Fabry-Perot interferometer model

Reactive scattering between molecules and atoms can be matched to the simple picture of an optical Fabry-Perot interferometer with two reflectors, M_1 and M_2 (Fig. 1). Mirror M_1 represents quantum reflection by the long-range vdW potential, and M_2 represents reflection near short range. Inelastic and reactive losses, which occur at close or short range (Fig. 1), are represented in the Fabry-Perot picture by transmission through the inner reflector M_2, followed by absorption. For an incoming flux I, the total transmission T_{tot} through both reflectors is given by

$$T_{tot} = \left(I \cdot |t_1|^2\right)\left(\frac{1-|r_2|^2}{|1-r_2 r_1 e^{-i\phi}|^2}\right) \equiv \left(I \cdot |t_1|^2\right)C \quad (1)$$

r_i and t_i are the amplitude reflection and transmission coefficients for mirror M_i, and ϕ is the round-trip phase, which, in the Fabry-Perot model, can be tuned by the distance between mirrors or the refractive index of the medium. The term $I \cdot |t_1|^2$ is the transmitted flux in the absence of the inner mirror (i.e., $r_2 = 0$) and, for collisions, represents the universal loss. The factor C represents the effect of interference. For later convenience, we characterize the inner reflection by a parameter $0 \le y \le 1$: $r_2 = (1-y)/(1+y)$, $t_2 = 2\sqrt{y}/(1+y)$, which is 1 for complete transmission and 0 for complete reflection. With $r_1 \sim 1$ (quantum reflection approaches unity at low energies), we obtain $C(y,\phi) = 2y/(1-\cos\phi + y^2(1+\cos\phi))$. Constructive interference at $\phi = 0$ leads to an enhancement $C = 1/y$, and destructive interference at $\phi = \pi$ leads to a minimum transmission with $C = y$. In the limit of small $y \ll 1$ relevant for our experimental results, the transmission probability for the inner mirror is ~$4y$.

In the case of cold collisions, scattering rates are periodic when the close-range potential is modified and new bound states are added to the interparticle potential. Each new bound state results in a resonance and "tunes" the Fabry-Perot interferometer over one full spectral range with the scattering length a varying by $\pm\infty$. In accordance with (*11*), we defined the normalized scattering length $s = a/\bar{a}$, where $\bar{a} = 0.47799 \cdot r_6$ is the mean scattering length (*34*). If we substitute $\cos\phi = 1 - 2/\left(1+(1-s)^2\right)$ (*35*), we obtain $C(y,s) = y\left(1+(1-s)^2\right)/\left(1+y^2(1-s)^2\right)$. This expression exactly reproduces the results of the quantum-defect model used in (*11*) for the imaginary part of the scattering length, $\beta = \bar{a}C(y,s)$, which is proportional to the zero-temperature loss-rate coefficient. Previous studies (*11*, *26*, *36*) already pointed out that their results can be interpreted as an interference effect of multiple reflections between short and long range. The relation between the phase shift ϕ and the parameter s exactly reflects how a short-range phase shift modifies the scattering length (*26*).

We extended this single-channel model (where s is the normalized background s-wave scattering length without loss, $y = 0$) by adding a Feshbach resonance as a lossless phase shifter for the Fabry-Perot phase

$$s(B) = q\left(1 - \frac{\Delta}{B - B_{res}}\right) \quad (2)$$

The resonance is at a magnetic field $B = B_{res}$, q characterizes the background scattering phase far away from the Feshbach resonance, and Δ is the width of the resonance. Tuning the magnetic field across the resonance takes the Fabry-Perot interferometer across a full spectral range and provides tunable interference at fixed low temperature. For finite collision energies, interference has been observed also as a function of collision energy (*37*).

Results and analysis

The measured loss rates for Na + NaLi collisions as a function of magnetic field are shown in Fig. 2. These data, which reveal a resonant enhancement of the loss by more than two orders of magnitude, represent the main result of this paper. Because the ratio of maximum and minimum loss is y^2 in the Fabry-Perot model, this result immediately suggested that

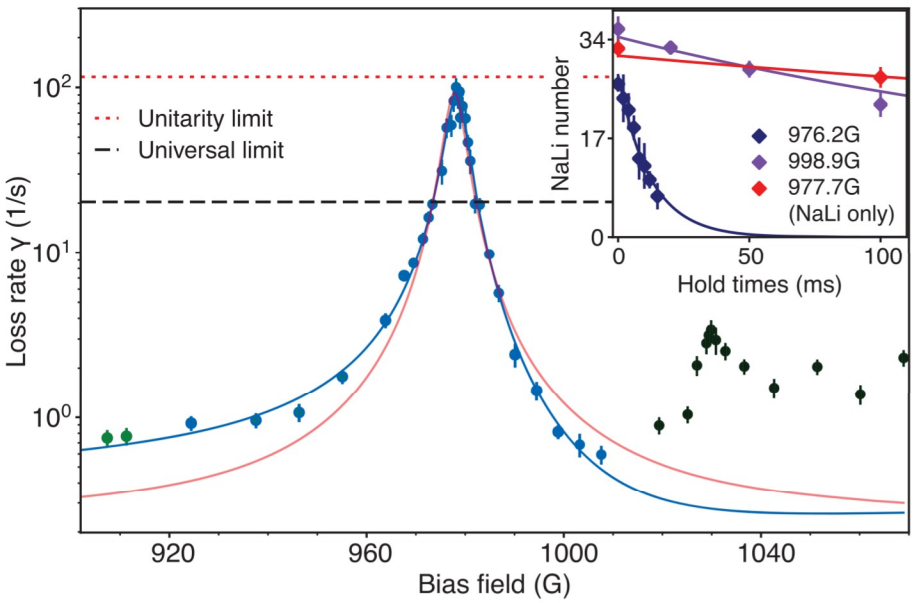

Fig. 2. Observation of Feshbach resonances in Na + NaLi collisions. Observed decay rates are shown as a function of bias field, with 100 Na atoms per pancake-shaped cloud at temperatures of T_{Na} = 1.60 μK and T_{NaLi} = 1.68 μK, corresponding to an overlap density of 1.1 × 10^{11} cm^{-3}. Data points taken with different sodium numbers and temperatures were scaled to the same overlap density (see SM). The blue line is a fit of the line shape to the Fabry-Perot contrast function *C*; the red line is a Lorentzian fit. Both fits use only the data points represented by blue circles. Green circles were excluded owing to another resonance near 880 G. Black circles show an additional resonance near 1030 G. The red dotted line is the unitarity limit in two dimensions for our experimental conditions. The black dashed line is the universal loss rate. Data points were acquired with 6 to 11 different hold times at each bias field; four to eight measurements at a given hold time were averaged. Error bars indicate 1 SD. The inset shows decay curves of molecules: The dark blue (or red) diamonds are near the strong resonance at 978 G with (or without) Na atoms, and the purple diamonds are off resonance near 1000 G with atoms. Relative to the dark blue diamonds, the overlap density of the purple data is larger by a factor of 2.2. The red line in the inset is a fit for the two-body molecular loss. The dark blue and purple lines are obtained by fitting the standard differential equations of two-body decay processes, including collisions with atoms (see SM).

y has to be <0.1. We could fit the asymmetric line shape of the resonance well to the function $C(y, s(B))$ with an overall normalization factor and obtain y = 0.05 and q = 1.61. However, the observed peak losses were close to the unitarity limit, which provides an upper limit for elastic and inelastic scattering rates. When the scattering length exceeds the de Broglie wavelength $\lambda\!\!\!^{-} = 1/k$ (where k is the relative wave number), the elastic cross section in 3D saturates at $4\pi\lambda\!\!\!^{-2}$, whereas the inelastic rate coefficient peaks at $(h/2\mu)\lambda\!\!\!^{-}$ (where h is Planck's constant). The observed peak loss rate was close to the unitarity limit, so we had to consider the role of nonzero momentum.

Combining the threshold quantum-defect model for the complex scattering length with a finite momentum S-matrix formulation for the scattering rates, Idziaszek and Julienne (*11*) obtained the complex scattering length

$$\tilde{a} = \bar{a}\left(s + y\frac{1+(1-s)^2}{i+y(1-s)}\right) \equiv \alpha - i\beta \quad (3)$$

where α is the real and $\beta = \bar{a}C(y, s(B))$ is the imaginary part of $\tilde{a}$. The loss-rate coefficient K is given by

$$K = f(k)\frac{2h}{\mu}\beta \quad (4)$$

The function $f(k) = (1 + k^2|\tilde{a}|^2 + 2k\beta)^{-1}$ establishes the unitarity limit for the scattering rates. So far, we have discussed inelastic scattering in three dimensions. However, because our atomic and molecular clouds had the shape of thin pancakes, we were in a 2D regime. Because the vdW length was much smaller than the thickness of the pancakes, the collisions were microscopically 3D and described by the 3D complex scattering length, but additionally, one had to use 2D scattering functions, leading to two effects. First, there is a logarithmic correction of the scattering length. For harmonic axial confinement with frequency ω_{ax}, the correction factor is $l = |(1 + (\tilde{a}/\sqrt{\pi}l_o)\ln(B\hbar\omega_{ax}/\pi k_B T))|^{-2}$, where $B \approx 0.915$ and $l_o = \sqrt{\hbar/\mu\omega_{ax}}$ is the associated oscillator length (*38*, *39*). Because Na and NaLi have different axial confinement frequencies ω_i and masses m_i, we used $\omega_{ax} = \mu(\omega_{Na}/m_{Na} + \omega_{NaLi}/m_{NaLi})$ (*40*). The correction factor l is large only at extremely low temperatures and near confinement-induced resonances (*38*, *39*). In our case, it provided a small shift of the peak loss by ~0.3 G. The second modification resulting from the 2D nature of the confinement is in the saturation factor, $f(k)$: In three dimensions, k is obtained from the thermal energy, whereas in two dimensions it is obtained from 2π times the relative kinetic energy of the zero-point motion, $k = \sqrt{\pi}/l_o$. The factor of 2π is a reminder that 2D dynamics cannot be fully captured by adding the zero-point energy to the thermal energy.

Our density calibration used the loss rate for collisions in a Na + NaLi mixture in a nonstretched spin state (see the "Experimental protocol" section). The loss rate is expressed by the imaginary part of the scattering length, β, and for the universal rate, $\beta = \bar{a}$.

For the ratio of the observed loss rate to the loss rate measured for the nonstretched state, we obtain

$$r(B) = f(k)l(\beta/\bar{a}) = \frac{\left|1 + (\tilde{a}/\sqrt{\pi}l_o)\ln\left(Bh^2/\pi\mu l_o^2 k_B T\right)\right|^{-2}}{1 + (\sqrt{\pi}/l_o)^2 l|\tilde{a}|^2 + 2(\sqrt{\pi}/l_o)l\beta}\left(\frac{\beta}{\bar{a}}\right) \quad (5)$$

The sodium density and all other factors are common mode and are canceled by taking the ratio. For the calibration measurement, $f(k)$ = 1 and l = 1, owing to the smallness of the scattering length.

We fit the loss-rate ratio $r(B)$ using four parameters: B_{res}, Δ, q, and y. Because the calibration measurements had uncertainties, we included a fifth fitting parameter in the form of an overall normalization factor, $\mathcal{N}$. We used an accurate theoretical value of $\bar{a}$ calculated for triplet ground-state NaLi + Na: $\bar{a} = 56.1a_0$ with ≲1.5% uncertainty (*33*). Figure 3 compares the experimental results with the fits. In the figure, we have multiplied $r(B)$ by the constant $2h\bar{a}/\mu$ and divided by the momentum-dependent 2D corrections $f(k)l$ calculated with the parameters of the best fit. In this way, we obtained the zero-temperature 3D loss-rate coefficient, $K_0(B) = (2h/\mu)\beta$, which is a microscopic property of the two-body system Na + NaLi.

The best fit with the single-channel model yielded B_{res} = 978.6(1) G, Δ = 28(2) G, y = 0.0094(47), and q = 1.60(7) with $\chi^2_{red} = 1.23$ [degrees of freedom (dof) = 27]. The normalization factor $\mathcal{N} = 1.32(45)$ was compatible with 1 and therefore was consistent with our calibration method.

Figure 3 also shows a weaker resonance near 1030 G. This resonance could not be explained by the single-channel model (i.e., with a lossless

phase shifter), which predicts that the maximum loss is larger than the universal limit. We therefore extended our model by considering a finite lifetime of the bound state coupled by the Feshbach resonance in the form of a linewidth Γ_b. This extension implied that the phase shifter of the Fabry-Perot resonator was now lossy and prevented the large resonant buildup of wave function inside the interferometer. In this two-channel model, we describe a lossy phase-shifter by

$$s_b(B) = q\left(1 - \frac{\Delta}{B - B_{res} - i\Gamma_b/2}\right) \quad (6)$$

With Eq. 6, we can express β in the Breit-Wigner form as in (*27*) (see SM). We assumed that y and q were the same as for the strong resonance because they characterized the same incoming channel, and we used the same normalization factor. We also included a slope and an offset as extra fit parameters to account for other loss channels not covered by our model. We obtained B_{res} = 1030.8(7) G, Δ = 0.21(4) G, and Γ_b = 5.38(4) G with $\chi^2_{red} = 2.4$ (dof = 10). The Δ parameter showed that the resonance at 1030 G was two orders of magnitude weaker than the one at 978 G. From the linewidth, we inferred the bound-state lifetime $\tau_b = (\delta\mu\Gamma_b)^{-1} \approx 60$ ns, where the relative magnetic moment between the entrance channel and the closed-channel bound state was $\delta\mu = 2\mu_B$ (where μ_B is the Bohr magneton) assuming a single spin-flip. In our study, the lifetime of a collision complex was obtained from a spectroscopic linewidth, whereas in all previous work on collisions of ultracold molecules, such lifetimes were obtained from a direct time-domain measurement (*9*, *10*). The short lifetime of the bound state suggests that the closed channel has a highly reactive doublet character. Some contribution to Γ_b and y could also come from the 1596-nm trapping light, which can excite collision complexes leading to loss, as observed in other molecular systems (*8*–*10*). However, given the small value of y, we expect this effect to be small.

We could also fit the strong resonance to the two-channel model and found Γ_b = 0 ± 1 G, confirming that we can regard the strong resonance as a lossless phase shifter. The longer lifetime of the closed channel associated with the strong resonance suggests that it is only weakly coupled to reactive channels. The difference between the two Feshbach resonances is highlighted by examining the total inelastic width, Γ_{inel}, of the resonance (see SM)

$$\Gamma_{inel} = \Gamma_b + \frac{2yq\Delta}{1 + y^2(q-1)^2} \quad (7)$$

where the first term is the natural linewidth of the bound state itself, and the second term represents the resonantly enhanced decay rate of the incoming channel. The width of the 978-G resonance was dominated by the open-channel losses at short range (i.e., $y \neq 0$), whereas the weak resonance was limited by the decay rate Γ_b. Equation 7 shows that the y parameter is more easily determined from a strong resonance. By contrast, the weaker resonance was insensitive to the short-range parameters y and q of the incoming channel. Figure 4 shows the real and imaginary parts of the scattering lengths for the two resonances and illustrates the power

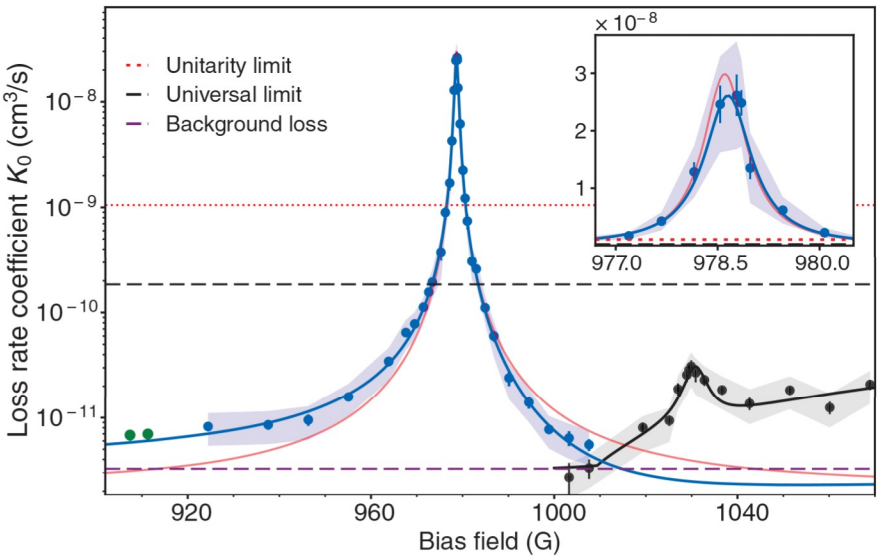

Fig. 3. Zero-temperature loss-rate coefficients K_0 for Na + NaLi collisions. K_0 is the imaginary part of the scattering length times $2h/\mu$. Experimental data points were corrected for nonzero momentum effects, $f(k)l$ (see the "Results and analysis" section). The blue line is the best fit based on the single-channel model; the red line is a symmetric Lorentzian fit. For both fits, only blue data points were included. The black line is a fit of the weak resonance using a two-channel model. The two black data points near 1005 G were obtained from the blue points by subtracting the contribution of the wings of the strong resonance. The red dotted line is the unitarity limit in two dimensions, $(h/2\mu)\sqrt{\pi}/l_0$. The black dashed line is the universal limit. The purple dashed line shows the background (open-channel) loss. The shaded area represents the total uncertainty, which is the quadrature sum of the standard deviation and the systematic uncertainty in the density calibration. The inset shows a magnified view of the central part of the figure on a linear scale.

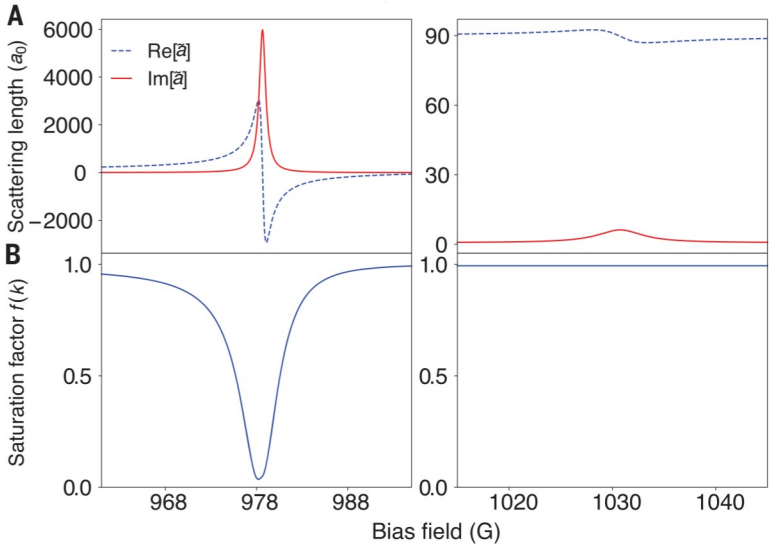

Fig. 4. Complex scattering length and saturation factor calculated from the best-fit results. (**A**) Real (Re) and imaginary (Im) parts of the scattering lengths $\tilde{a}$ near the strong resonance calculated according to the single-channel model (left plot) and near the weak resonance calculated according to the two-channel model (right plot). (**B**) Saturation factor $f(k)$ with $k = \sqrt{\pi}/l_0$, where l_0 is the oscillator length for the effective axial confinement frequency. The saturation was negligible for the weak resonance (right plot), whereas $f(k)$ ~ 0.03 at the strong resonance (left plot).

of the simple model: Analysis of the inelastic scattering provides a full description of all s-wave scattering properties, including elastic scattering and momentum dependence. We can also calculate the good-to-bad collision ratio, $k(\alpha^2+\beta^2)/\beta$, and find that it is maximized away from the resonance (see SM).

Figure 3 shows that the zero-momentum loss rate could be tuned over four orders of magnitude and exceeded the universal limit by a factor of 100, which was reduced by the unitarity limit to a factor of 5 (Fig. 2) [see also (*41*)].

The quality factor of the Fabry-Perot resonator becomes smaller for nonzero momentum, owing to the lower long-range quantum reflectivity, which has a threshold law of $|r_1| \approx 1-2\bar{a}k$. This relation yields $|r_1| \sim 0.93$ using the total (i.e., thermal and zero-point) momentum for k. The resonant enhancement inside the Fabry-Perot resonator is reduced when the transmission of the outer mirror (M_1) is comparable to that of the inner mirror (M_2)—i.e., when $\bar{a}k \sim y$. At this point, the unitarity saturation takes effect and reduces the loss rate from its zero-temperature value shown in Fig. 3.

Discussion

In this study, we have demonstrated the substantial suppression and enhancement of reactive collisions relative to the universal limit, which is possible only if $y \ll 1$, and we have achieved control of chemical reactions via external magnetic fields. An asymmetric line shape can lead to a suppression of inelastic losses below the background loss (*42*). This suppression was not realized for the results shown in Fig. 3, owing to the neighboring weaker Feshbach resonance.

Our analysis highlights the conditions necessary to observe such a high dynamic range tunability of reactive collisions. The possible contrast is given by $1/y^2$ but is only realized if the Feshbach resonance is sufficiently strong and coupled to a sufficiently long-lived state: $q\Delta/\Gamma_b > 1/y$. This condition for the Feshbach resonance is more difficult to fulfill for smaller values of y, but the Na + NaLi system satisfies this condition for the resonance at 978 G and for several other resonances that we have observed but not yet fully analyzed.

The models for reactive collisions presented here may look rather specialized. However, our two-channel model captures the low-temperature limit of the most general resonance possible for which the complex scattering length is represented by a circle in the complex plane (*27*, *43*) (see SM).

Universal reaction rates are determined only by quantum reflection of the long-range potential and do not provide any information about the "real chemistry" at short range. Therefore, discovery and characterization of nonuniversal molecular systems are major goals of the field (*15*–*17*, *20*, *21*, *44*). However, most of the cases studied exhibited only two- to fourfold deviation from the universal limit, and interpretation of these cases required an accurate density calibration that was not always performed. Some studies showed inelastic rates well below the universal limit, without any resonances (*45*–*47*), which can provide only an upper bound for y and leave q undetermined. This work has demonstrated how short-range reflectivity makes it possible to access information about short-range interactions and collisional intermediate complexes. Our analysis showed that suppression of loss below the universal limit could occur for a wide range of parameters, but strong enhancement of loss beyond the universal limit requires fine tuning: an almost lossless Fabry-Perot interferometer tuned to resonance.

In this work, we have experimentally validated a method on the basis of external magnetic fields and quantum interference to realize quantum control of chemistry. Previous studies used microwaves (*44*, *48*) or electric fields (*49*) to control losses in molecular systems with strong long-range dipolar interactions by modifying the universal rate limit. In our study, we used magnetic fields and quantum interference, without the need for dipolar interactions, to achieve loss-rate coefficients that far exceed the universal limit. All of these methods control one specific decay channel. With the weak resonance, we have also demonstrated that magnetic field can switch between two different mechanisms of reactive scattering, occurring in the chemically stable incoming and the lossy closed channels, respectively.

REFERENCES AND NOTES

1. S. Inouye *et al.*, *Nature* **392**, 151–154 (1998).
2. C. Chin, R. Grimm, P. Julienne, E. Tiesinga, *Rev. Mod. Phys.* **82**, 1225–1286 (2010).
3. A. B. Henson, S. Gersten, Y. Shagam, J. Narevicius, E. Narevicius, *Science* **338**, 234–238 (2012).
4. T. de Jongh *et al.*, *Science* **368**, 626–630 (2020).
5. L. D. Carr, D. DeMille, R. V. Krems, J. Ye, *New J. Phys.* **11**, 055049 (2009).
6. Y. Liu *et al.*, *Nature* **593**, 379–384 (2021).
7. M. Mayle, B. P. Ruzic, J. L. Bohn, *Phys. Rev. A* **85**, 062712 (2012).
8. A. Christianen, M. W. Zwierlein, G. C. Groenenboom, T. Karman, *Phys. Rev. Lett.* **123**, 123402 (2019).
9. P. D. Gregory, J. A. Blackmore, S. L. Bromley, S. L. Cornish, *Phys. Rev. Lett.* **124**, 163402 (2020).
10. Y. Liu *et al.*, *Nat. Phys.* **16**, 1132–1136 (2020).
11. Z. Idziaszek, P. S. Julienne, *Phys. Rev. Lett.* **104**, 113202 (2010).
12. R. V. Krems, *Int. Rev. Phys. Chem.* **24**, 99–118 (2005).
13. M. T. Bell, T. P. Softley, *Mol. Phys.* **107**, 99–132 (2009).
14. S. Ospelkaus *et al.*, *Science* **327**, 853–857 (2010).
15. J. W. Park, S. A. Will, M. W. Zwierlein, *Phys. Rev. Lett.* **114**, 205302 (2015).
16. X. Ye, M. Guo, M. L. González-Martínez, G. Quéméner, D. Wang, *Sci. Adv.* **4**, eaaq0083 (2018).
17. P. D. Gregory *et al.*, *Nat. Commun.* **10**, 3104 (2019).
18. T. Takekoshi *et al.*, *Phys. Rev. Lett.* **113**, 205301 (2014).
19. L. W. Cheuk *et al.*, *Phys. Rev. Lett.* **125**, 043401 (2020).
20. B. Drews, M. Deiß, K. Jachymski, Z. Idziaszek, J. Hecker Denschlag, *Nat. Commun.* **8**, 14854 (2017).
21. G. Polovy, E. Frieling, D. Uhland, J. Schmidt, K. W. Madison, *Phys. Rev. A* **102**, 013310 (2020).
22. E. R. Hudson, N. B. Gilfoy, S. Kotochigova, J. M. Sage, D. DeMille, *Phys. Rev. Lett.* **100**, 203201 (2008).
23. N. Zahzam, T. Vogt, M. Mudrich, D. Comparat, P. Pillet, *Phys. Rev. Lett.* **96**, 023202 (2006).
24. P. Staanum, S. D. Kraft, J. Lange, R. Wester, M. Weidemüller, *Phys. Rev. Lett.* **96**, 023201 (2006).
25. J. Deiglmayr *et al.*, *J. Phys. Conf. Ser.* **264**, 012014 (2011).
26. M. D. Frye, P. S. Julienne, J. M. Hutson, *New J. Phys.* **17**, 045019 (2015).
27. J. M. Hutson, *New J. Phys.* **9**, 152 (2007).
28. X.-Y. Wang *et al.*, *New J. Phys.* **23**, 115010 (2021).
29. H. Yang *et al.*, arXiv:2104.11424 [physics.atom-ph] (2021).
30. H. Son, J. J. Park, W. Ketterle, A. O. Jamison, *Nature* **580**, 197–200 (2020).
31. T. M. Rvachov *et al.*, *Phys. Rev. Lett.* **119**, 143001 (2017).
32. B. Gao, *Phys. Rev. Lett.* **105**, 263203 (2010).
33. R. Hermsmeier, J. Kłos, S. Kotochigova, T. V. Tscherbul, *Phys. Rev. Lett.* **127**, 103402 (2021).
34. G. F. Gribakin, V. V. Flambaum, *Phys. Rev. A* **48**, 546–553 (1993).
35. This expression is equivalent to $\tan(\phi/2) = 1/(1-s)$, which is also given in (*26*).
36. Y.-P. Bai, J.-L. Li, G.-R. Wang, S.-L. Cong, *Phys. Rev. A* **100**, 012705 (2019).
37. Y. Xie *et al.*, *Science* **368**, 767–771 (2020).
38. D. S. Petrov, G. V. Shlyapnikov, *Phys. Rev. A* **64**, 012706 (2001).
39. Z. Idziaszek, K. Jachymski, P. S. Julienne, *New J. Phys.* **17**, 035007 (2015).
40. Although the relative motion is no longer a simple harmonic oscillator, the expression for ω_{ax} provides the correct kinetic energy $\hbar\omega_{ax}/4$ of the relative motion.
41. In (*50*), Yang *et al.* mention a resonant loss rate two to three times the universal limit. However, this is based on an estimate for the universal limit and an unspecified density calibration. Our weak resonance shows that it is easily possible to observe Feshbach resonances that do not exceed the universal limit.
42. J. M. Hutson, M. Beyene, M. L. González-Martínez, *Phys. Rev. Lett.* **103**, 163201 (2009).
43. R. A. Rowlands, M. L. Gonzalez-Martinez, J. M. Hutson, arXiv:0707.4397 [physics.chem-ph] (2007).
44. L. Anderegg *et al.*, *Science* **373**, 779–782 (2021).
45. S. Jurgilas *et al.*, *Phys. Rev. Lett.* **126**, 153401 (2021).
46. K. K. Voges *et al.*, *Phys. Rev. Lett.* **125**, 083401 (2020).
47. T. T. Wang, M.-S. Heo, T. M. Rvachov, D. A. Cotta, W. Ketterle, *Phys. Rev. Lett.* **110**, 173203 (2013).
48. Z. Z. Yan *et al.*, *Phys. Rev. Lett.* **125**, 063401 (2020).
49. K. Matsuda *et al.*, *Science* **370**, 1324–1327 (2020).
50. H. Yang *et al.*, *Science* **363**, 261–264 (2019).
51. H. Son *et al.*, Data of: Control of reactive collisions by quantum interference, version 1, Zenodo (2021); https://doi.org/10.5281/zenodo.5797536.

ACKNOWLEDGMENTS

We thank D. Petrov, P. Julienne, K. Jachymski, and T. Tscherbul for valuable discussions. **Funding:** We acknowledge support from the NSF through the Center for Ultracold Atoms (grant no. 1506369) and from the Air Force Office of Scientific Research (MURI, grant no. FA9550-21-1-0069). Some of the analysis was performed by W.K. at the Aspen Center for Physics, which is supported by the NSF (grant PHY-1607611). H.S. and J.J.P. acknowledge additional support from the Samsung Scholarship. **Author contributions:** H.S. and J.J.P. carried out the experimental work. All authors contributed to the development of models, data analysis, and writing the manuscript. **Competing interests:** None declared. **Data and materials availability:** All data needed to evaluate the conclusions in the paper are present in the main paper or the supplementary materials. All data presented in this paper are deposited at Zenodo (*51*).

SUPPLEMENTARY MATERIALS

science.org/doi/10.1126/science.abl7257
Supplementary Text
Figs. S1 and S2
References (*52*–*57*)

5 September 2021; accepted 23 December 2021
10.1126/science.abl7257

Science

Control of reactive collisions by quantum interference

Hyungmok SonJuliana J. ParkYu-Kun LuAlan O. JamisonTijs KarmanWolfgang Ketterle

Science, 375 (6584), • DOI: 10.1126/science.abl7257

Magnetic control of chemistry

There is a considerable interest in realizing control of molecular reactions at ultracold temperatures because of unprecedented opportunities in the ultimate quantum regime. Son *et al*. discovered an ideal system, a sodium atom and a sodium–lithium molecule, in which the combination of Feshbach resonances and low short-range loss probability allows for the significant suppression or enhancement of reactive collisions, controlled by external magnetic fields (see the Perspective by Cornish and Hutson). This work presents a method for manipulating the reactivity of ultracold molecules that is qualitatively different from previous experiments. At the same time, this method is highly dependent on the distinctive short-range properties offered by the sodium/sodium–lithium complex and is subject to further testing in other systems. —YS

Science (ISSN) is published by the American Association for the Advancement of Science. 1200 New York Avenue NW, Washington, DC 20005. The title *Science* is a registered trademark of AAAS.